Aging Cell

WILEY

RESEARCH ARTICLE OPEN ACCESS

Resilience to Cardiac Aging in Greenland Shark *Somniosus microcephalus*

Elena Chiavacci[1] | Kirstine Fleng Steffensen[2] | Pierre Delaroche[3] | Emanuele Astoricchio[4] | Amalie Bech Poulsen[2] | Daniel Brayson[5] | Fulvio Garibaldi[6] | Luca Lanteri[6] | Christian Pinali[3] | Giovanni Roppo Valente[6] | Federico Vignati[6] | John Fleng Steffensen[2,†] | Holly Shiels[3] | Eva Terzibasi Tozzini[4] | Alessandro Cellerino[1,7]

[1]Biology Laboratory (BIO@SNS), Scuola Normale Superiore, Pisa, Italy | [2]Marine Biological Section, Department of Biology, University of Copenhagen, Helsingør, Denmark | [3]Division of Cardiovascular Sciences, School of Medical Sciences, Faculty of Biology, Medicine and Health, University of Manchester, Manchester, UK | [4]Biology and Evolution of Marine Organisms Department (BEOM), Stazione Zoologica Anton Dohrn, Napoli, Italy | [5]School of Life Sciences, University of Westminster, London, UK | [6]Dipartimento di Scienze Della Terra, Dell'ambiente e Della Vita – DISTAV, Università di Genova, Genova, Italy | [7]Fritz Lipmann Institute for Age Research, Leibniz Institute, Jena, Germany

Correspondence: Alessandro Cellerino (alessandro.cellerino@sns.it)

Received: 12 December 2025 | **Revised:** 20 March 2026 | **Accepted:** 2 April 2026

Keywords: Cardiac Aging | Fibrosis | Greenland shark | Lipofuscin | *Somniosus microcephalus*

ABSTRACT

The Greenland shark (*Somniosus microcephalus*), with a lifespan estimated around 300 years, represents a unique model for studying vertebrate longevity. Here, we characterize its cardiac aging profile and compare it with two other species: the deep-sea shark *Etmopterus spinax* and the short-lived teleost *Nothobranchius furzeri*. Histological analysis revealed extensive interstitial and perivascular fibrosis throughout the ventricular myocardium of *S. microcephalus*, affecting both compact and spongy layers of both sexes. This fibrotic pattern was absent in *E. spinax* and *N. furzeri*, suggesting it is a specific feature of *S. microcephalus*. We also observed extreme lipofuscin accumulation within cardiomyocytes of *S. microcephalus*, which correlates at the ultrastructural level with the abundance of damaged mitochondria and the presence of strikingly enlarged lysosomes filled with electrondense material of likely mitochondrial origin. Additionally, in the myocardium of *S. microcephalus* we found abundant deposition of the oxidative stress marker 3-nitrotyrosine. Remarkably, despite showing multiple canonical markers of aging such as fibrosis, lipofuscin accumulation, and oxidative stress, *S. microcephalus* individuals appeared healthy and physiologically uncompromised at the time of capture. These findings suggest that *S. microcephalus* has evolved resilience to molecular and tissue-level aging signs and hallmarks, supporting sustained cardiac function over centuries and offering new insights into the mechanisms of extreme vertebrate longevity.

1 | Introduction

The Greenland shark (*Somniosus microcephalus*) is a giant (> 5 m) shark living in deep, cold water in high northern latitudes. It is characterized by slow growth rate (~1 cm/year) and exceptional longevity. Radiocarbon dating of eye lens nuclei revealed that sexual maturity is reached at ~150 years and a maximum lifespans of at least 272 years, with the largest animal (502 cm) estimated to be 392 ± 120 years old, making it the slowest maturing, longest-living known vertebrate (Hansen 1963; Nielsen et al. 2016). *S. microcephalus* is a sluggish swimmer, with average cruising speed of ~0.3 m/s and ~9 tail beats per minute, with possibly little capacity for sustained high-speed swimming (Compagno et al. 2005; Nielsen et al. 2016; Watanabe et al. 2012). When corrected for body size, the Greenland shark exhibits the slowest sustained swim

†Deceased.

speed and tail-beat frequency recorded among known fishes (Watanabe et al. 2012) matched by a low metabolism (Ste-Marie et al. 2022). Despite its remarkable longevity, knowledge of life history, ecology and physiology of this charismatic and elusive animal is very limited (MacNeil et al. 2012; Costantini et al. 2017; Herbert et al. 2017). Given the preeminent contribution of cardiovascular function to general mortality risk (Visseren et al. 2021; Vlachopoulos et al. 2010; Timmis et al. 2024; Townsend et al. 2022), a particularly interesting question is how heart function can be maintained for centuries in this species. In humans and most vertebrates, aging is characterized by apparent histological changes in the hearts, including cardiac fibrotic remodeling, loss of cardiomyocyte reserve, and cumulative oxidative stress, all of which contribute to the heart functional decline (Biernacka and Frangogiannis 2011; Lu et al. 2017; Fleg and Strait 2012; Yoneyama et al. 2016; Anversa and Nadal-Ginard 2002; Gazoti Debessa et al. 2001; Chen et al. 2022; Lesnefsky et al. 2016). Recently, spatial RNA sequencing in old mouse heart reveals a clear picture of the age-related changes in gene expression toward a fibrotic cardiac phenotype, while proteomics data showed an increase of reactive oxygen species (ROS) and a concomitant decline in antioxidant defenses which exacerbate the oxidative stress (Basilicata et al. 2025). It remains unknown whether *S. microcephalus* is spared by such age-related cardiac remodeling and related functional consequences. Some characteristics of the Greenland shark's heart and blood vessels have only recently begun to emerge. *S. microcephalus* has a two-chambered heart typical of Chondrichthyans, and consists of sinus venosus, atrium, ventricle and outflow tract arranged sequentially, pumping blood to the gills for oxygenation before circulating it through the body (Shadwick et al. 2018). *S. microcephalus* cardiocirculatory system may exhibit specific physiological and structural adaptations to its sluggish lifestyle that makes it resistant to age-dependent remodeling, thereby enabling its extreme longevity. An alternative possibility is that *S. microcephalus* maintains its cardiac function despite age-dependent remodeling thereby showing resilience.

In the present study, we set to discriminate between these two possibilities and investigated histological aging signs and hallmarks in *S. microcephalus* heart specimens. We also analyzed hearts of two key comparison species: the deep-sea shark *Etmopterus spinax* (Linnaeus, 1758) and the short-lived African turquoise killifish (*Nothobranchius furzeri*). *E. spinax*, commonly known as the velvet belly lantern shark, distributed widely across the northeast Atlantic Ocean and the Mediterranean Sea (Compagno 1984; Aranha et al. 2009). Both *E. spinax* and *S. microcephalus* derive from a common Squalomorph ancestor that lived ~100 Mya and colonized deep-sea habitats (Straube et al. 2015), but *E. spinax* is of minute size (< 50 cm) and wild-capture records indicate maximum lifespans of ~8 years for males and ~11 for females (Gennari and Scacco 2007; Coelho and Erzini 2008), making it a valuable comparative model for distinguishing traits specifically associated with exceptional lifespan from general deep-sea adaptations. *N. furzeri* is the vertebrate with the shortest captive lifespan and is an emerging vertebrate model in aging research due to its compressed lifespan and expression of all the key hallmarks of mammalian aging (Cellerino et al. 2016; Di Cicco et al. 2011). Moreover, it serves as a key reference for cardiac aging in a poikilothermic aquatic vertebrate (Ahuja et al. 2019).

Lipofuscin is an autofluorescent pigment composed primarily of cross-linked oxidized proteins, lipids, and metals. It shows a yellow-brown specific chromatic signal under fluorescent light and accumulates progressively in postmitotic cells over time. Lipofuscin is widely recognized as a hallmark of cellular aging (Terman and Brunk 1998, 2006; Brunk and Terman 2002; Malkoff and Strehler 1963; Kakimoto et al. 2019). In *N. furzeri*, lipofuscin age-related accumulation was employed as an aging marker in the liver (Ng'oma et al. 2014; Terzibasi et al. 2009), brain (Terzibasi et al. 2008; Terzibasi Tozzini et al. 2013), and heart (Ahuja et al. 2019). The heart of *N. furzeri* is structurally analogs to that of zebrafish *Danio rerio*, which consists of a thin outer cortical layer and is essentially made of trabeculated myocardium, while Elasmobranchs exhibit a mixed myocardial organization combining spongy and well-developed compact layers (Sánchez-Iranzo et al. 2018; López-Unzu et al. 2024; Fukuda et al. 2019). Furthermore, recently, *N. furzeri* has also been proposed as a valuable model for studying cardiac aging (Ahuja et al. 2019; Ma et al. 2025). Aged *N. furzeri* exhibits accumulation of 3-nitrotyrosine (3-NT), another well-established biomarker of aging due to oxidative and nitrosative stress (Heid et al. 2017). In rat models, 3-NT levels rise progressively with age, with elevated 3-NT levels linked to impaired SERCA2a function, mitochondrial destabilization, and endothelial dysfunction, even in the absence of overt cardiovascular disease (Knyushko et al. 2005), this is consistent with a gradual disruption in redox homeostasis during physiological cardiac aging. Similarly, NT-3 was found increased in aged *N. furzeri* healthy hearts, indicating 3-NT as a reliable marker of cardiac aging (Heid et al. 2017). Thus, we included the aged teleost model *N. furzeri* as a natural comparative model to the exceptionally long-lived Chondrichthyan *S. microcephalus*. The comparison of the three species *S. microcephalus*, *E. spinax*, and *N. furzeri* allowed us (i) to validate the lipofuscin and 3-NT accumulation as new cardiac aging markers in *S. microcephalus* heart; (ii) to distinguish *S. microcephalus* features of cardiac aging associated with centenary lifespan versus adaptations associated with deep-sea habitat or phylogenetic lineage.

2 | Materials and Methods

2.1 | Tissues Sampling and Processing

For paraffin embedding and Electron microscopy (EM) *S. microcephalus* heart samples were collected from six *S. microcephalus*, that were captured by long-line fishing in Greenland waters (Table S1), this methodological choice carries relevant behavioral and functional implications: (i) the animals were able to detect and correctly identify bait in the natural environment, and (ii) they actively pursued and captured it. These behaviors require intact sensory processing, motor coordination, and sufficient physiological performance, and therefore provide indirect evidence of preserved organismal function. Hearts were dissected immediately post-mortem and 1 cm ×1 cm size piece of myocardium taken from myocardial

surface until lumen, mid way down the ventricle between the apex and base, recovered in 4% paraformaldehyde (PFA), fixed for 48 h, then PBS washed and dehydrated trough ethanol (EtOH) 25%, 50%, 70% series. For EM: compact and spongy myocardium tissues were sampled separately. *E. spinax* heart samples were collected from seven specimens classified as juveniles (Follesa and Carbonara 2019) (Table S2) captured by deep-water trawlers operating in the Ligurian Sea (Santa Margherita Ligure). Hearts were dissected and processed as described for *S. microcephalus*. *N. furzeri* heart samples were collected from three females and three males of MZM-0410 strain at 39 weeks of age. Animals were euthanized with Tricaine, MS-222, in accordance with the prescription of the European Union (Directive 2010/63/UE) and hearts dissected and fixed in 4% PFA overnight (O.N.). Samples were PBS washed and dehydrated through EtOH series. All paraffin samples were sectioned 6 μm thin.

2.2 | Masson's Trichrome Staining

Masson's trichrome staining (Bioptica) was performed on deparaffinized sections according to routine procedures for light microscopy with the following modifications: nuclei were stained with Weigert's Iron Hematoxylin Solution for 10 min and then glass slides H_2O washed before proceeding with Masson's trichrome staining.

2.3 | Cardiac Fibrosis Quantification

For the fibrosis quantification we analyzed three animals for each species, two males and one female for *S. microcephalus* and two female and one male *for E. spinax*. For each animal three different field of Masson's trichrome stainings were imaged in the spongy and compact myocardium layer in white light, all images were captured under identical illumination, exposure, and white balance settings to maintain consistency across samples. Images were acquired using an epifluorescence microscope (Nikon EclipseE600) equipped with a DS-Fi3 color camera (Nikon, Tokyo, Japan) and handled with Gimp v2.10. For the analysis, Images were converted to the Hue–Saturation–Brightness (HSB) color space, and the channels were thresholded to generate binary masks for total tissue area (Hue 125–255, Saturation 0–255, Brightness 104–255) and collagen-positive regions (Hue 0–255, Saturation 0–255, Brightness 225–227). These thresholds were empirically selected to reliably capture collagen-positive staining while excluding nuclei, background signal, and non-specific staining artifacts Logical and combination of thresholded HBS channels yielded a binary fibrosis mask representing collagen-positive areas. Pixel counts were obtained using standard ImageJ measurement tools, and fibrosis was quantified as the percentage ratio of collagen-positive area to total tissue area (collagen/total area). Lumen and pericardial regions were excluded from the total tissue mask during image processing For each animal, values obtained from multiple imaging fields were first averaged to generate a single animal-level mean, and all statistical comparisons were performed using these animal-level values. Data were analyzed and plotted with GraphPad Prism (version 6.1, GraphPad Software, San Diego, CA, USA) as mean ± SEM for each animal, statistical comparisons between two groups were performed using an unpaired Student's *t*-test.

2.4 | Sudan Black B Staining

Deparaffinized sections were stained in Sudan B black (Sigma Aldrich, Cat # S0395) 0.5% solution for 10 min RT, and washed three times in H_2O 10 min.

2.5 | Photobleaching

Deparaffinized slices were stained with Hoechst 33,342 2 μM 1:10 000 for 5 min, washed three times in PBS. Images were acquired using an epifluorescence microscope (Nikon EclipseE600) equipped with a DS-Fi3 color camera (Nikon, Tokyo, Japan). Photobleaching was performed exposing the samples to continuous fluorescence blue-light illumination (DAPI filter) for 30 min.

2.6 | Lipofuscin Quantification

For lipofuscin quantification we analyzed three females for each species. For each animal three different fields were imaged within the spongy myocardium layer with an epifluorescence microscope in the DAPI channel. Fluorescence images were analyzed using Fiji (ImageJ, NIH, version 1.54p) as follows: nuclei were identified in the DAPI channel using a semi-automated macro workflow. Images were first converted to 8-bit grayscale, nuclei were segmented by automatic thresholding (Otsu method) followed by binarization and separation of touching objects using the *Watershed* algorithm. Nuclei were quantified using the *Analyze Particles* tool. All processing parameters were kept constant across samples. Nuclei masks were then generated and their fluorescence subtracted from the corresponding image. The resulting nuclei-subtracted image was then analyzed over the entire field and the mean gray value recorded. For each animal, values obtained from multiple imaging fields were first averaged to generate a single animal-level mean, and all statistical comparisons were performed using these animal-level values. Data were analyzed and plotted with GraphPad Prism (version 6.1, GraphPad Software, San Diego, CA, USA) as mean ± SEM for each animal; statistical comparisons between two groups were performed using an unpaired Student's *t*-test. Masson's trichrome, Sudan Black B staining, photobleaching, and lipofuscin were imaged with an epifluorescence microscope (Nikon EclipseE600) equipped with a DS-Fi3 color camera (Nikon, Tokyo, Japan). Images were handled with Gimp v2.10. DAPI channel-based approach, combined with color camera acquisition and masking, ensures that the quantified signal corresponds specifically to lipofuscin.

2.7 | Electron Microscopy (EM)

Tissues were immediately excised post mortem, immersed in Karnovsky fixative (2.5% glutaraldehyde, 2% PFA in 0.1 M sodium cacodylate buffer, pH 7.2–7.4) (Pinali and Kitmitto 2014),

cut into ~1 mm^3 cubes, and stored at 4°C until further processing. Samples were post-fixed and stained en bloc following a protocol adapted for cardiomyocytes (Deerinck et al. 2010; Smith and Starborg 2019). After washing in 0.1 M sodium cacodylate buffer, samples were post-fixed in reduced osmium (2% osmium tetroxide, 1.5% potassium ferrocyanide) for 1 h, rinsed in double-distilled water (ddH_2O), incubated in filtered thiocarbohydrazide for 1 h at RT, and washed again in ddH_2O. They were subsequently treated with 1% osmium tetroxide for 1 h, washed, incubated in 1% uranyl acetate overnight at 4°C, washed, and finally incubated in Walton's lead aspartate at 60°C for 30 min before a final rinse in ddH_2O. Dehydration was carried out through graded EtOH (30%, 50%, 70%, 90%, 100% and 100%) followed by pure acetone. Samples were infiltrated with increasing concentrations of TAAB 812 Hard Resin (TAAB Laboratories Equipment Ltd., UK) in acetone (25% resin in acetone, 50%, 75% up to 100% resin) and polymerized at 60°C for 24–48 h. Resin blocks were mounted on aluminum pins, trimmed to expose a 500 μm × 500 μm face, polished with a diamond knife, and gold-coated prior to imaging. Volumetric imaging was performed using an FEI Quanta 250 FEG scanning electron microscope (FEI Company, USA) equipped with a Gatan 3View serial block-face system (Gatan Inc., USA). Image stacks were acquired at 3.8 kV, 0.45 Torr chamber pressure, and 3.5 μs/pixel dwell time, at a calibrated magnification of 12 nm/pixel. Serial sections of 50 nm were cut, producing image stacks of several hundred slices at 6000 × 6000 pixels. The resulting voxel dimensions were 12 nm (x, y) and 50 nm (z).

2.8 | 3D Reconstructions

Automatic segmentation of SBF-SEM data was performed using Dragonfly 3D World software version 2024.1. For preprocessing, a volume containing a large autophagosome identified in the compact ventricular myocardium of the 434 cm female was extracted from the original SBF-SEM dataset using IMOD's trimvol command (Kremer et al. 1996). The resulting MRC file was imported into Dragonfly, where six slices were manually annotated for the autophagosome and mitochondria using the ROI Painter tools. A convolutional neural network with a U-Net architecture (Ronneberger et al. 2015) was trained using Dragonfly's Deep Learning Tool. To enhance dataset diversity, a two-fold data augmentation was applied (vertical/horizontal flips, rotations up to 180°, shear up to 2°, and scaling between 90% and 110%). Training used 128 × 128 patches, a batch size of 32, stride ratio and learning rate of 1.0, Adadelta optimization, and Categorical Cross-Entropy loss. The model trained for 500 epochs, achieving a Dice score > 0.95 and validation loss < 0.05. Segmentation of the complete dataset was performed using Dragonfly's Segment with AI feature, followed by manual correction of mislabelled voxels. Autophagosome volume was automatically computed by the software. Movies were generated using Dragonfly's Movie Maker (3D views) and 2D Animation panels.

2.9 | Immunohistochemistry (IHC)

Immunohistochemistry was carried out according to standard procedures. Primary antibodies were all incubated overnight at 4°C according to the following dilutions: sarcomeric α-actinin (Sigma Cat# A7811) 1:400, 3-nitrotyrosine 3-NT (Invitrogen Cat# A-21,285) 1:200, lysosomal Lamp1 (Kelmer Sacramento et al. 2020) (Abcam Cat# ab24170) 1:500. After the incubation, sections were washed three times in PBS 1× and incubated for 2 h with secondary antibodies 1:500 (Invitrogen polyclonal rabbit Alexa Fluor 488 Conjugated Cat# A-11,008, RRID:AB_143165; Invitrogen polyclonal mouse Alexa Fluor 568, Cat# A-11,004). Nuclei were stained with Hoechst 1:5000 for 5 min and sections were mounted with fluoroshield mounting medium. Negative controls omitting the primary antibody were run in parallel with all IHC. IHC Imaging was performed using a confocal STELLARIS 8 (Leica) microscope and operated via LAS X software (Leica Microsystems, Wetzlar, Germany). High-resolution Airyscan imaging was performed with a confocal Zeiss LSM900 microscope (Carl Zeiss) equipped with Airyscan 2 and operated via ZEN 3.1 (blue edition) software. Images were handled with Gimp v2.10.

2.10 | TUNEL Assay

TUNEL assay was performed according to manufacturer protocol, and positive controls were performed accordingly with DNAse I treatment: Click-iT TUNEL Colorimetric IHC Detection Kit cat. C10625. Images were handled with Gimp v2.10.

3 | Results

3.1 | Cardiac Fibrosis

We started our investigation by assessing the histology of the *S. microcephalus* ventricle. The ventricular morphology of *S. microcephalus* is consistent with that of low-activity elasmobranchs, characterized by a rigid outer pericardial layer predominantly composed of collagen (Figure S1), and a compact myocardial layer overlying a widespread spongy myocardium. Additionally, a well-developed coronary artery network supplying the entire ventricle is present (Figure S1). Masson's trichrome staining revealed widespread fibrosis throughout the ventricular myocardium of *S. microcephalus*, affecting both the external compact layer and the internal spongy myocardium, belonging to the interstitial and perivascular fibrosis subtype (Figure 1A–F, Figure S2A–C). We analyzed ten *S. microcephalus* ranging 300–390 cm TL. The size corresponds roughly to 100–155 years and the time of sexual maturity in females (Nielsen et al. 2016). Collagen infiltration was observed in all ten specimens and affected both myocardial sublayers and both sexes (Figure 1A–F). To exclude that extensive collagen deposition is a general trait associated with the pressure found in deep-sea environment, we performed histological analysis of the ventricular myocardium of the deep-sea squaliform shark *Etmopterus spinax*. Masson's trichrome staining of *E. spinax* ventricular wall revealed a canonical shark myocardial architecture, with an outer fibrotic pericardial layer underlaid by compact and spongy myocardial layer. No evidence of cardiac fibrosis was detected in the ventricular wall of either females or males in a total of seven specimens (Figure 1G–L). Quantification of fibrotic tissue in the two sharks, two males and one female for *S. microcephalus*

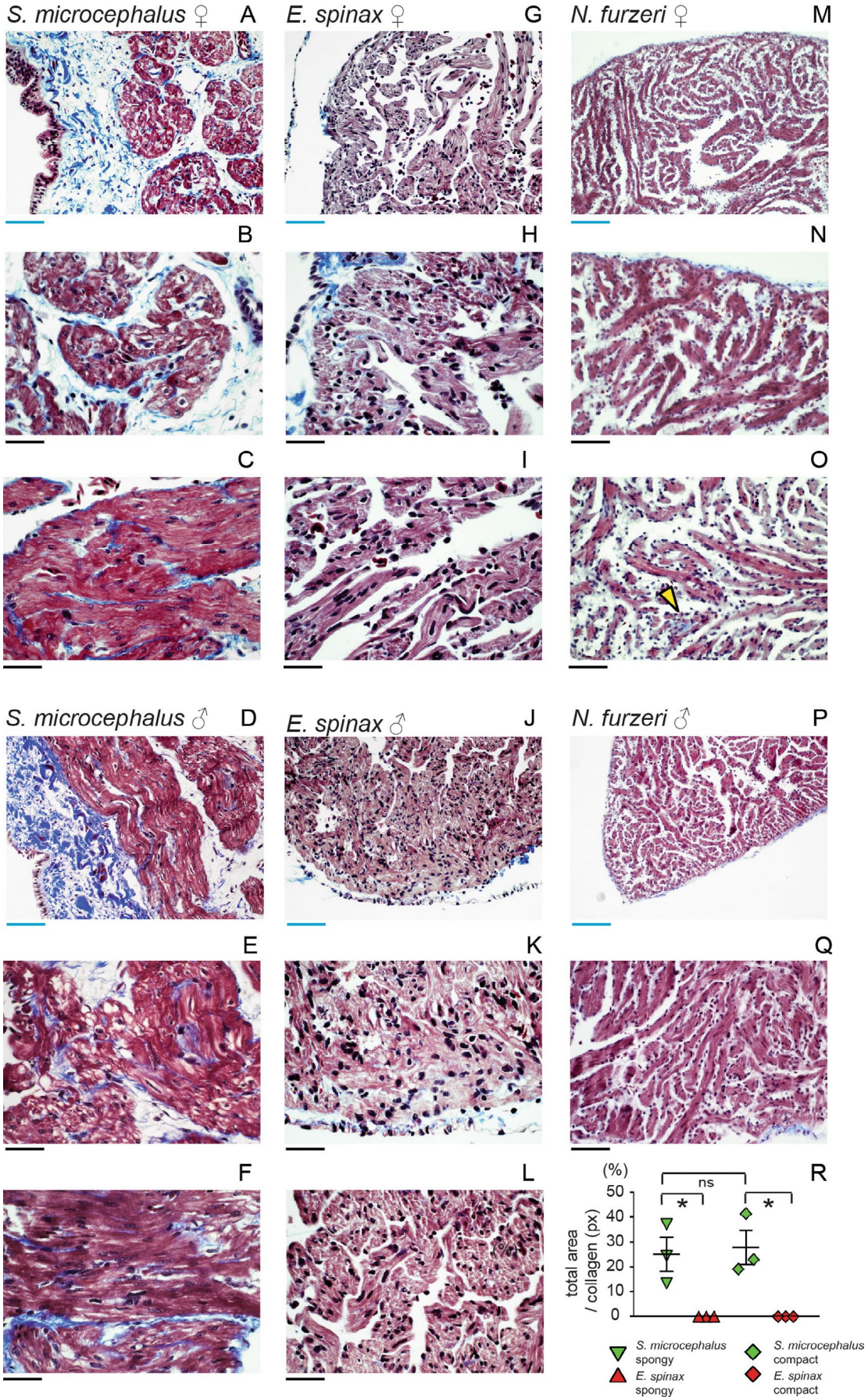

FIGURE 1 | Legend on next page.

FIGURE 1 | Histological evaluation and cardiac fibrosis of several fish species. (A, B) *S. microcephalus* 341 cm TL female, compact layer. (C) *S. microcephalus* 341 cm TL female, spongy layer. (D, E) *S. microcephalus* 335 cm TL male. (F) *S. microcephalus* 335 TL male, spongy layer. (G, H) *E. spinax* 300 mm TL female, compact layer. (I) *E. spinax* 300 mm TL female, spongy layer. (J, K) *E. spinax* 260 mm TL male, compact layer. (L) *E. spinax* 260 mm TL male, spongy layer. (M–O) *N. furzeri* ventricular myocardium, 39 weeks old female. (P, Q) *N. furzeri* ventricular myocardium, 39 weeks old male. Blue scalebar: 100 μm, black scalebar: 50 μm. yellow arrow: Ischemic collagen scar. (R) Quantification of cardiac fibrosis in sharks. $^{*}p < 0.05$.

and two female and one male for *E. spinax*, clearly showed the absence of cardiac fibrosis both in compact and spongy myocardium of *E. spinax*; while the *S. microcephalus* showed a statistically significative massive fibrotic presence in both layers (Figure 1R, Figures S3A–C and S4A,B). To further determine if the massive cardiac interstitial fibrosis is a general phenotypic characteristic of aged fish, or it is specific of the extremely long-living *S. microcephalus*, we performed histological analysis of the ventricular myocardium of two males and one female at 39 weeks of age (i.e., median lifespan) of the short living teleost *N. furzeri*, a model where age-dependent cardiac changes are well described (Ahuja et al. 2019; Heid et al. 2017; Ma et al. 2025). We did not detect interstitial cardiac fibrosis (Figure 1M–Q) but observed occasionally cardiac scars reminiscent of ischemic lesions (two males and one female of the samples evaluated), a representative lesion is illustrated in Figure 1O, yellow arrow. The presence of such scars highlights the capability of killifish myocardium to generate collagen rich fibrotic scars when focally injured, thus excluding that absence of interstitial fibrosis is due to inability to mount a fibrotic injury response. To exclude the possibility that the ten *S. microcephalus* individuals had underlying non-physiological cardiac conditions at the time of capture and did not suffer from acute cardiac injury as consequence of the capture technique, we performed a TUNEL assay on myocardial sections. No apoptotic or necrotic cells were detected compared to the positive controls, both in compact neither spongy myocardial layers, indicating that the animals exhibited an healthy myocardial tissue (Figure S5A–Y).

3.2 | Lipofuscin Accumulation

To explore whether extreme longevity of *S. microcephalus* correlates with expression of cellular aging biomarkers, we analyzed lipofuscin deposition in the ventricular wall of *S. microcephalus*, *E. spinax* and aged *N. furzeri*. Sudan Black B staining of ventricular myocardial sections revealed massive and diffuse lipofuscin accumulation filling the entire cardiomyocyte in *S. microcephalus*, both in the compact and spongy myocardial layers, in ten animals, females and males (Figure 2A–F, Figure S4C,D). In contrast, the seven *E. spinax* animals exhibited limited Sudan Black–positive areas, primarily restricted to localized regions of the compact myocardium (Figure 2G–L), and with markedly lower staining intensity as compared to *S. microcephalus*. Interestingly, the six aged *N. furzeri* showed abundant lipofuscin granules, although these were detectable only at higher magnification and did not fill the sarcoplasm of the cardiomyocytes. Unlike in sharks, the pigment was localized mainly outside the cardiomyocytes, dispersed within the trabecular interspaces (Figure 2M–P, black arrows). To confirm lipofuscin accumulation, we exploited its intrinsic autofluorescence, which typically emits across the green-to-red spectrum (approximately 540–640 nm) (Terman and Brunk 1998). Comparative autofluorescence analysis of myocardial sections from *S. microcephalus*, *E. spinax*, and aged *N. furzeri* revealed the characteristic yellow-brown autofluorescence of lipofuscin granules under blue-light excitation (DAPI filter). In *S. microcephalus*, prominent lipofuscin accumulation was observed within cardiomyocytes of both the compact and spongy myocardial layers, in specimens of both sexes (Figure 3A–D; Figure S4E,F). By contrast, no apparent lipofuscin autofluorescence was detected in *E. spinax* (Figure 3E–H) even though autofluorescence of erythrocytes was readily visible in both species (Figure 3D,F; red arrows). As expected, lipofuscin quantification between *S. microcephalus* and *E. spinax* highlighted a statistically significant difference in lipofuscin content between the two shark species (Figure 3K). As previously assumed, aged *N. furzeri* displayed numerous yellow-brown autofluorescent granules, consistent with lipofuscin, located primarily within the trabecular interspaces rather than inside cardiomyocytes (Figure 3I,J). Given the Sudan Black B well-documented ability to quench lipofuscin's intrinsic autofluorescence, we extended our analysis by imaging *S. microcephalus* and aged *N. furzeri* myocardial sections stained with Sudan Black B under fluorescence light across three major spectral channels: blue (DAPI filter), green (GFP/FITC filter), and red (TRITC/CY3 filter). As anticipated, *S. microcephalus* samples exhibited marked attenuation of yellow-brown autofluorescence in the blue spectrum (Figure 4A), confirming Sudan Black B-mediated quenching, while dense deposits of Sudan Black B-positive lipofuscin remained visible (Figure 4B,C) under white light. To further validate that the observed autofluorescence originated from lipofuscin, we conducted a photobleaching experiment, capitalizing on the well-documented resistance of lipofuscin to photobleaching (Sun and Chakrabartty 2016; Davies et al. 2001). Myocardial sections were exposed to continuous blue-light illumination (DAPI filter) for 30 min. Following exposure, we observed marked photobleaching of the nuclear Hoechst staining (Figure 4D,E), confirming effective light-induced degradation of canonical fluorophores. By contrast, the strong yellow-brown autofluorescent signal attributed to lipofuscin persisted within cardiomyocytes and remained clearly visible post-bleaching (Figure 4F), consistent with lipofuscin's photostability. As expected, in the aged heart of *N. furzeri*, photobleaching revealed an abundance of persistent yellow-brown autofluorescent granules localized predominantly in the trabecular interspaces, further supporting their identification as lipofuscin (Figure 4G). Moreover, the *N. furzeri* accumulation of lipofuscin outside the cardiomyocytes is in line with what was already observed in mice hearts (Wang et al. 2022). These granules remained detectable in the far-red fluorescence channel of a confocal microscope,

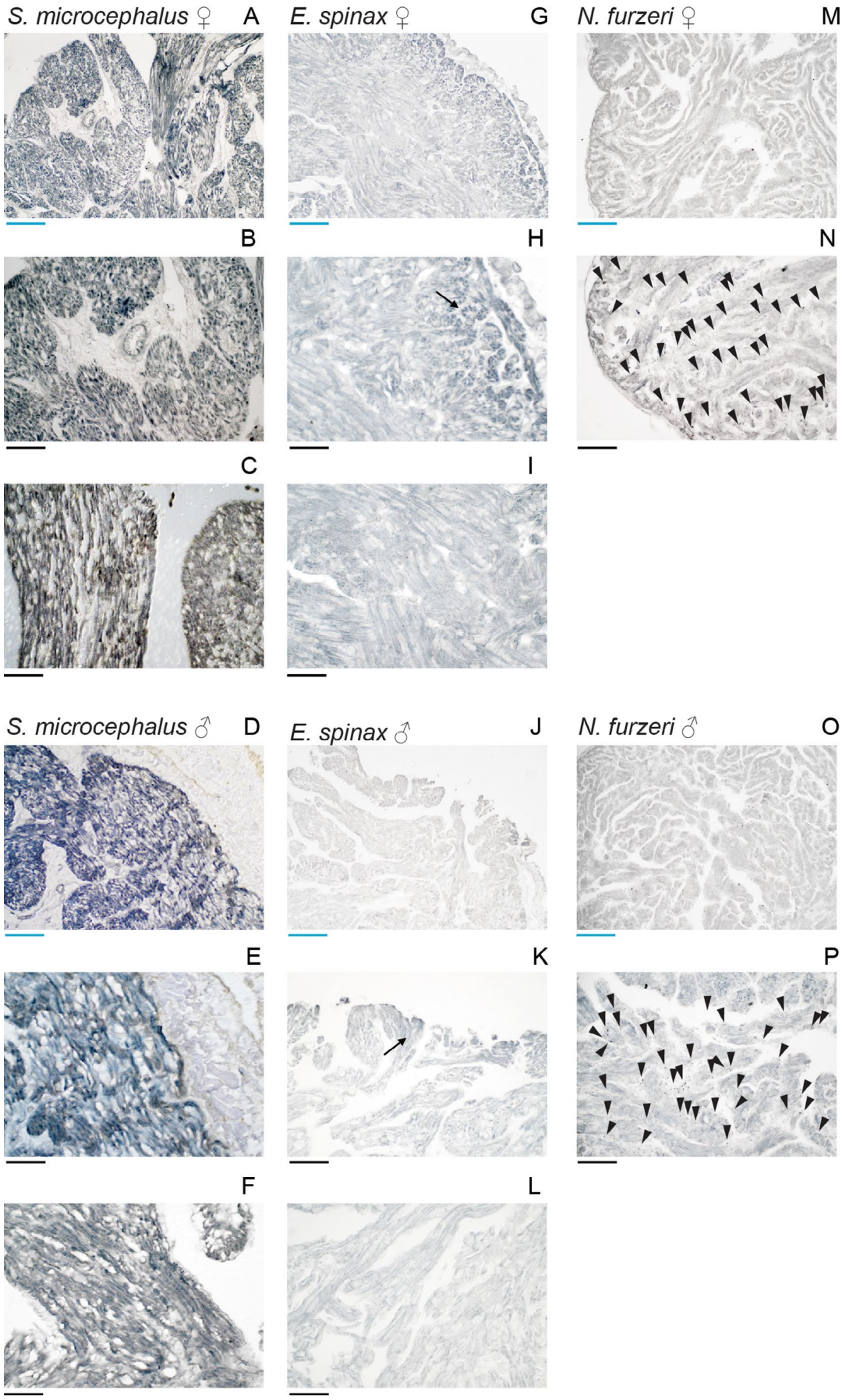

FIGURE 2 | Legend on next page.

FIGURE 2 | Sudan Black B staining of ventricular myocardium. (A, B) *S. microcephalus* 341 cm TL female, compact layer. *S. microcephalus* female, compact layer. (C) *S. microcephalus* 341 cm TL female, spongy layer. (D, E) *S. microcephalus* 310 cm TL male. (F) *S. microcephalus* 310 cm TL male, spongy layer. (G, H) *E. spinax* 300 mm TL female, compact layer, black arrow. (I) *E. spinax* 300 mm TL female, spongy layer. (J, K) *E. spinax* 260 mm TL male, compact layer, black arrow. (L) *E. spinax* 260 mm TL male, spongy layer. (M, N) *N. furzeri* 39 weeks old ventricular myocardium, female, lipofuscin granules, black triangles. (O, P) *N. furzeri* 39 weeks old ventricular myocardium 39 weeks old male, lipofuscin granules, black triangles. Blue scalebar: 100 μm, black scalebar: 50 μm.

further supporting their identification based on lipofuscin's broad emission spectrum and resistance to photobleaching (Figure 6S,V).

3.3 | Ultrastructural Analysis

To further investigate the subcellular nature of lipofuscin accumulation, we performed electron microscopy (EM) of the *S. microcephalus* myocardial compact layer. Lipofuscin is a by-product of lipid peroxidation that accumulates within lysosomes as an indigestible amorphous aggregate. Damaged mitochondria, due to oxidative stress, are one of the main sources of the oxidized material that becomes lipofuscin and accumulates into autophagosomes (Terman et al. 2004; König et al. 2017; Lu et al. 2020). We analyzed three *S. microcephalus* specimens (one male and two females) ranging from 294 to 434 cm TL. In all specimens, we observed a massive accumulation of electrondense, lipofuscin-packed autophagosomes (Figure 5A–E, white arrows), together with numerous lysosomes filled with electrondense material (Figure 5A–E, red arrows). These were embedded within a dense network of mitochondria. In addition, we identified degenerating mitochondria apparently in the process of being phagocytosed and incorporated into autophagosomes (Figure 5B–E, yellow arrows). The autophagosomes exhibited variable morphology and size, ranging from mitochondrion-like profiles (Figure 5B,E, white arrows) to structures several micrometers in size (Figure 5A,C,D, white arrows). A three-dimensional (3D) reconstruction of one such autophagosome revealed an exceptionally large volume of 24 μm^3 (Video S1), supporting the hypothesis that lipofuscin can accumulate within *S. microcephalus* cardiomyocytes in very large amounts without compromising their viability or functionality. To further confirm ultrastructural data, we performed high-resolution Airyscan imaging on *S. microcephalus* compact and spongy myocardial layers of a 341 cm TL female, 335 cm TL male, and 390 TL female to image lysosomal and lipofuscin granules. Single-plane acquisitions showed (i) myocardial lipofuscin distribution consistent with Sudan Black B staining in both the compact and spongy myocardium of the three animals analyzed (Figures 4B–C, 5F–U, Figure S4G–N); (ii) the granular-shape nature of the lipofuscin structures, consistent with EM data (Figure 5F,G,I–K,M–O,Q–S,U; Figure S4G,H,J–L,N); (iii) the general colocalization of lysosomal Lamp1 with the lipofuscin granules (Figure 5G–I,K–M,O–Q,S–U; Figure S4H–J,L–N). Colocalization is variable in Lamp1 fluorescence intensity (Figure 5F–U, single examples in G, K, O, S: orange arrows; Figure S4G–N), and some lipofuscin structures are Lamp1 negative (Figure 5F–U, single examples in G, K, O, S: violet arrows; Figure S4G–N), while lipofuscin-negative lysosomes are clearly distinguishable all around the myocardium (Figure 5G,K,O,S; Figure S4G–N), indicating the specificity and the robustness of the IHC staining. Together, the EM and IHC findings support the hypothesis that the large autophagosomes represent fusion products of lysosomes with degenerating mitochondria.

3.4 | 3-Nirotyrosine Accumulation

3-Nitrotyrosine (3-NT), a stable product of tyrosine nitration by reactive nitrogen species, is widely recognized as a biomarker of cardiac aging and a reliable biomarker of oxidative and nitrosative stress. Its accumulation has been reported in cardiac tissue across several species, including the *N. furzeri* (Heid et al. 2017). We investigated 3-NT presence in the ventricular myocardium of *S. microcephalus*, *E. spinax* and aged *N. furzeri*. Strong immunoreactivity for 3-NT (Figure 6A–H) was detected in both male and female specimens in the ventricular myocardium of *S. microcephalus*, with prominent staining observed in both the compact (Figure 6A,B) and spongy myocardial layers (Figure 6E,F). Autofluorescence imaging in the far-red channel confirmed the presence of lipofuscin within cardiomyocytes, consistent with earlier observations (Figure 6A,D,E,H). In contrast, *E. spinax* myocardial tissue showed no detectable 3-NT signal (Figure 6I–R) and lacked lipofuscin-associated autofluorescence (Figure 6I,L,M,P). Interestingly, nuclei within the spongy myocardium of *E. spinax* appeared enlarged as compared to those of the other species analyzed (Figures 1H,I,K,L, 3B,D,F,H and 6M), suggesting a species-specific morphological trait. Notably, in *S. microcephalus*, 3-NT deposition was particularly abundant in interstitial regions, whereas its presence within cardiomyocytes was comparable to that observed in aged *N. furzeri* (Figure 6Q–T) and already reported in the literature (Heid et al. 2017).

4 | Discussion

Our study provides the first histological and molecular analysis of cardiac aging in the Greenland shark (*Somniosus microcephalus*), a species notable for its extraordinary lifespan. Human centenarians show three different phenotypes: some show no (escapers) or delayed (escapers) onset of age-associated diseases; others maintain physiological functions despite the presence of pathological conditions (survivors). These conditions are exemplary of resistance vs. resilience. Resistance is the capacity to oppose a perturbation; resilience can be defined as the capacity of a system to return to a physiological state after a perturbation. Despite harboring signs of cardiac aging such as interstitial and perivascular fibrosis, lipofuscin accumulation, and 3-NT deposition, *S. microcephalus* individuals appeared phenotypically healthy. This unique potential dissociation of aging markers

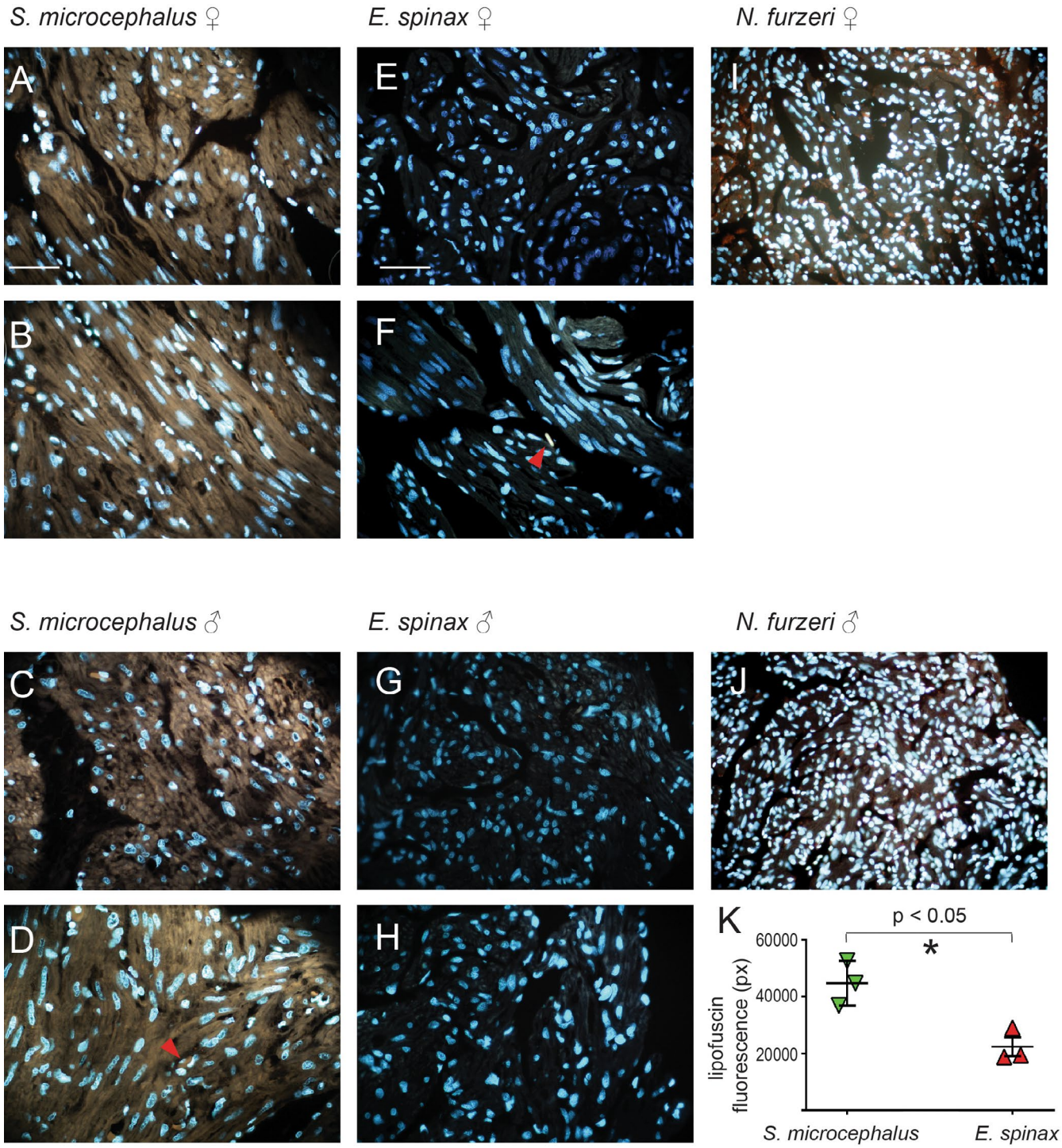

FIGURE 3 | Myocardium autofluorescence highlighting lipofuscin. (A) *S. microcephalus* 325 cm TL female, myocardial compact layer. (B) *S. microcephalus* 325 cm TL female, myocardial spongy layer. (C) *S. microcephalus* 310 cm TL male, myocardial compact layer. (D) *S. microcephalus* 310 cm TL male, myocardial spongy layer. (E) *E. spinax* 300 mm TL female, myocardial compact layer. (F) *E. spinax* 300 mm TL female, myocardial spongy layer. (G) *E. spinax* 260 mm TL male, myocardial compact layer. (H) *E. spinax* 260 mm TL male, spongy layer. (I) *N. furzeri* ventricular myocardium 39 weeks old female. (J) *N. furzeri* 39 weeks old ventricular myocardium, male. (K) lipofuscin quantification in *S. microcephalus* and *E. spinax*. *$p < 0.05$.

from functional decline underscores resilience as a key mechanism enabling extreme longevity and highlights the Greenland shark as a unique model for studying resilience to tissue aging.

In our analysis we observed extensive interstitial and perivascular fibrosis in the ventricles of *S. microcephalus*, spanning both the compact and spongy myocardial layers. Cardiac fibrosis is a well-documented sign of aging across vertebrate taxa, including humans, rodents, and teleosts, and is generally associated with maladaptive remodeling, reduced diastolic compliance, and increased risk of arrhythmogenesis (Schulman et al. 1992; Gazoti Debessa et al. 2001; Levy et al. 1988; Chen et al. 2022; Kane

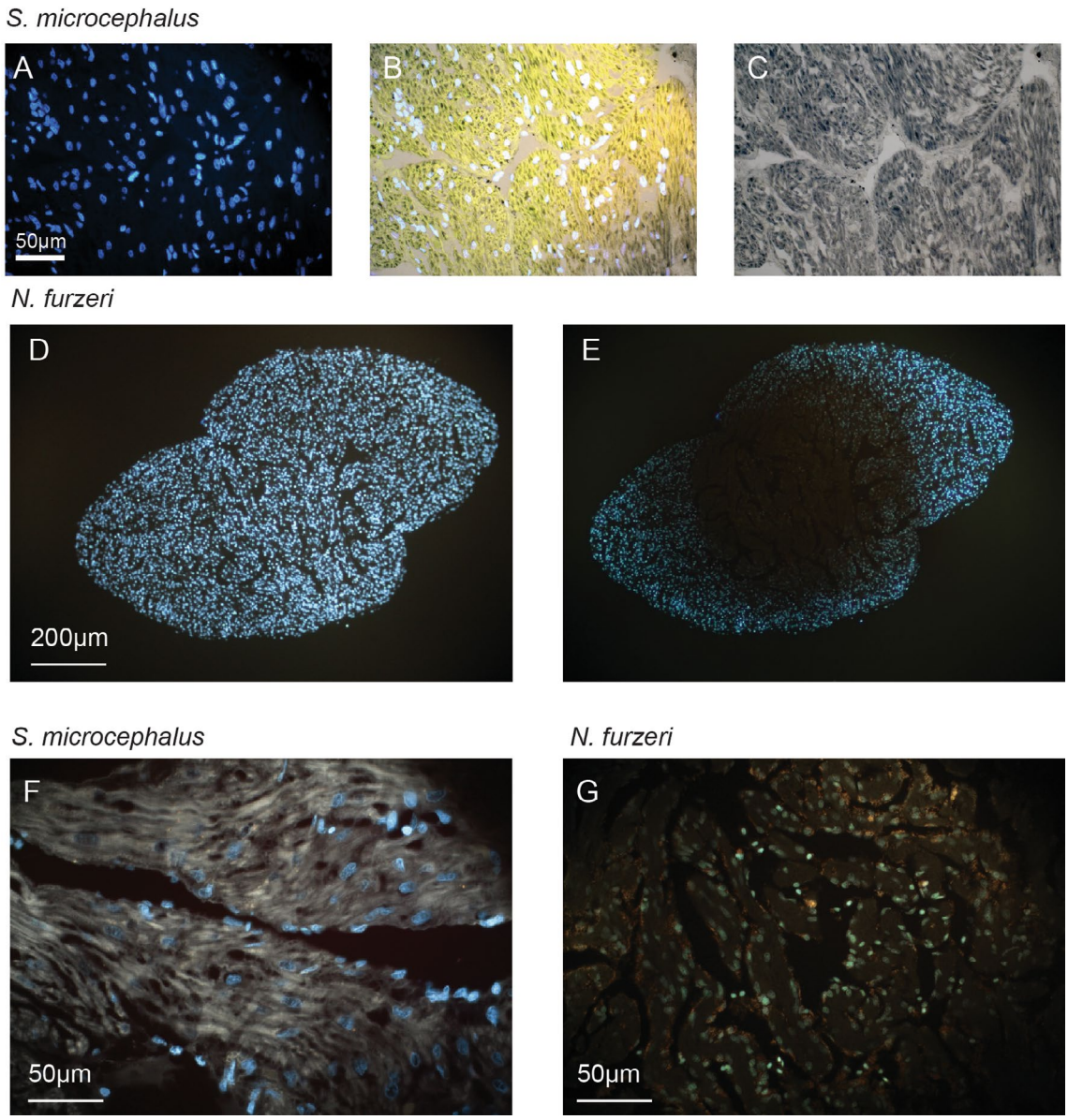

FIGURE 4 | Lipofuscin in the ventricular myocardium. (A) Sudan Black B stained ventricular myocardium of *S. microcephalus*, acquired with DAPI-filter fluorescent light showed quenched lipofuscin autofluorescence, with Hoechst in blue. (B) RGB autofluorescence acquired in the TRITC/CY3, GFP/FITC and DAPI filters, respectively and merged on the white light acquisition. Sudan Black B granules quenched the RGB yellow-resulting basal autofluorescence. (C) White light acquisition. Representative images of coronal section of *N. furzeri* ventricle before (D, E) after photobleaching. (F) Photobleached acquisition of a spongy ventricular *S. microcephalus* section shows clear yellow-brown autofluorescence. (G) Photobleached acquisition of *N. furzeri* ventricle shows clear yellow-brown autofluorescence granules. (A, B, D–G) cyan: Hoechst acquired with DAPI-filter. (A, D–G) yellow-brown: Lipofuscin autofluorescence acquired with DAPI-filter.

et al. 2021; Dai and Rabinovitch 2009; Keen et al. 2015). Age-associated cardiac fibrosis is typically interstitial and diffuse, rather than focal or replacement in nature. Histologically, it is marked by an accumulation of collagen type I and type III, predominantly in the interstitial and perivascular regions (Biernacka and Frangogiannis 2011). Surprisingly, this fibrotic signature was not accompanied by any morphological abnormalities at the time of sampling in the adult examined individuals of *S. microcephalus*, confirmed by absence of TUNEL- positive cells in the myocardium of all of them (Figure S5). These findings are consistent with recent reports of non-pathological, age-related cardiac fibrosis in mice, described as a sign of cardiac aging (Basilicata et al. 2025). Notably, neither the deep-sea elasmobranch *E. spinax* nor the aged teleost *N. furzeri* displayed comparable fibrotic remodeling. The absence of fibrosis in *E. spinax*, a species that inhabits comparable deep-sea environments but exhibits a markedly shorter lifespan, suggests that the extensive fibrosis observed in *S. microcephalus* is not simply an adaptive response to hydrostatic pressure. On the other hand, the absence of interstitial fibrosis in the aged heart of *N. furzeri* support the hypothesis that aging processes alone are not sufficient to develop collagen deposition and interstitial fibrosis formation. Rather, our observations support the fashinating hypothesis that *S. microcephalus* has evolved an exceptional resilience to age-related cardiac fibrosis, maintaining physiological function despite extensive extracellular matrix remodeling. In the Mediterranean

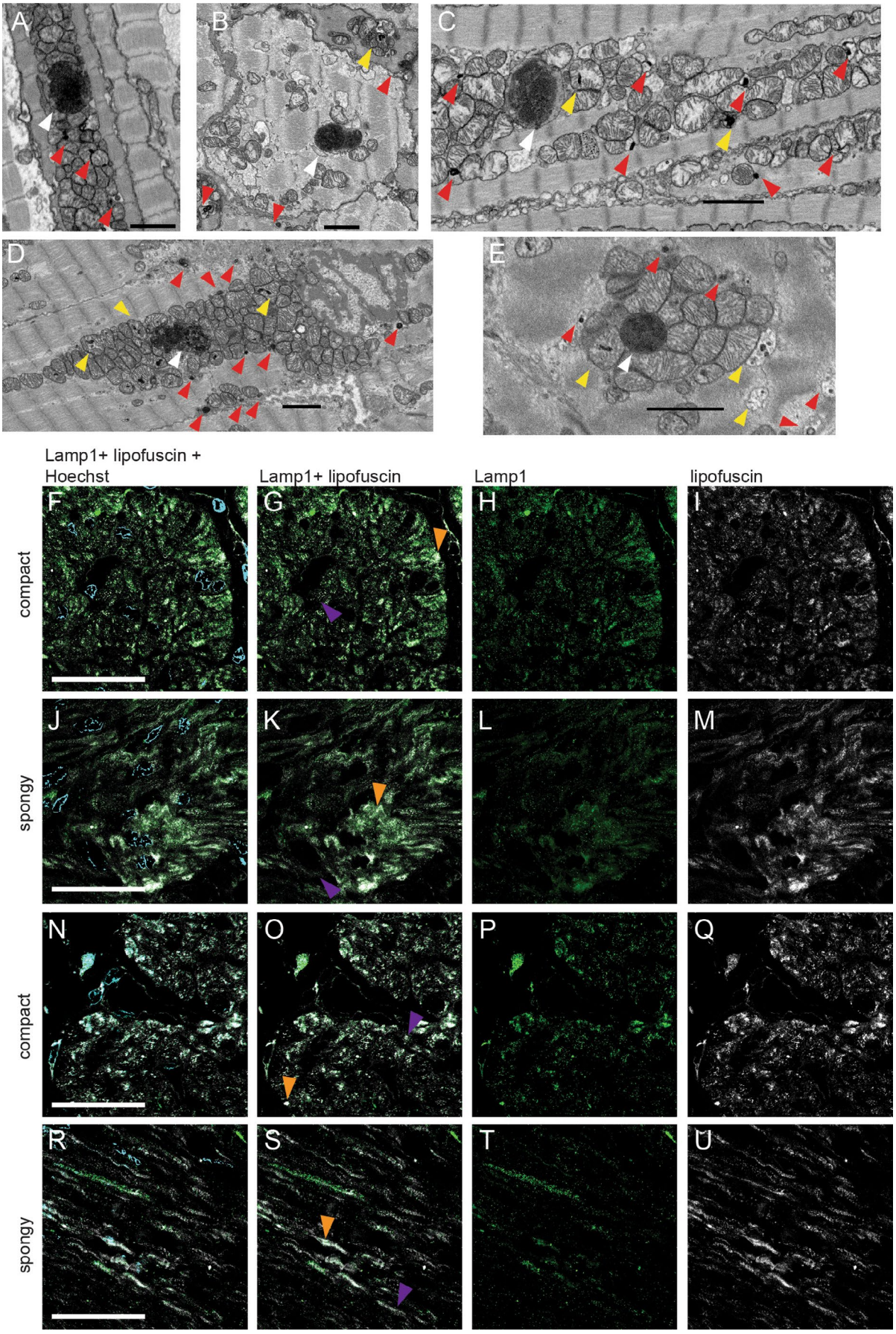

FIGURE 5 | Legend on next page.

FIGURE 5 | EM of *S. microcephalus* showing lipofuscin accumulation. (A–D) EM of a 294 cm male. (E, F) EM of a 310 cm female. (G, H) EM of a 434 cm female. White arrow: Autophagosomes. Red arrow: Lysosomes. Yellow arrow: Dying mitochondria in the process to be incorporated inside autophagosomes. IHC of *S. microcephalus* showing lysosomes and lipofuscin accumulation acquired with Airyscan. (F–M) IHC of 341 cm TL female myocardium. (N–U) IHC of 335 cm TL male myocardium. Orange arrows: Single examples of lysosomal Lamp1 and lipofuscin colocalization. Purple arrows: Single examples of lipofuscin granules. Cyan: Hoechst. Green: Lamp1. White: Lipofuscin. Black scalebar: 2 μm, white scalebar: 50 μm.

Sea, the deep-water temperature structure is comparatively stable, with a persistent thermocline and typical temperatures of approximately 12.8°C–13.2°C below ~200 m depth (Houpert et al. 2015; Cardin et al. 2015). In several teleost freshwater species, including, common carp *Cyprinus carpio* (Goolish 1987), channel catfish *Ictalurus punctatusi* and green sunfish *Lepomis cyanellus* (Kent et al. 1988) chronic cold acclimation has been shown to induce cardiac ventricular hypertrophy. In anadromous salmonids such as rainbow trout *Oncorhynchus mykiss* and atlantic salmon *Salmo salar*, cold-induced cardiac fibrosis has also been documented (Farrell et al. 1988; Keen et al. 2015). Such cold-associated cardiac remodeling in teleosts is generally interpreted as an adaptive response, producing a hypertrophied ventricle capable of generating the necessary contractile force to maintain hemodynamic function at low temperatures while limiting overstretch under conditions of increased blood viscosity in species which can not reduce physical activity during seasonal temperature changes. For reference, *O. mykiss* typically exhibits arterial blood pressures of ~3–6 kPa and resting heart rates of 20–50 bpm (Le Mével et al. 2002), whereas *S. salar* shows values of ~4–7 kPa and ~56 bpm (Perry et al. 1999). Blood pressure in Greenland sharks has never been directly measured, still it has been estimated by analyzing the relative amounts of elastin and collagen in the wall of the ventral aorta, together with measuring its compliance characteristics over a range of pressures (Shadwick et al. 2018). These data suggest that the Greenland shark's average blood pressure is approximately 2.3–2.8 kPa (Shadwick et al. 2018), much lower than other sharks. For example the *Scyliorhinus canicula* (commonly known as small spotted catsharks) is an animal with a relatively low activity and metabolic rate, still possess a blood pressure of 3–5 kPa (Taylor et al. 2003). Other sharks (e.g., lamnid sharks) have even higher metabolism and blood pressure, over > 7 kPa (Lai et al. 1997). Such comparatively low blood pressure in *S. microcephalus* may reduce the selective pressure for cold-induced ventricular stiffening or fibrosis. To date, cold-induced cardiac hypertrophy or fibrosis has not been documented in Elasmobranchs, suggesting that this form of thermal cardiac remodeling may represent an evolutionary adaptation specific to teleost fishes, particularly those inhabiting freshwater or anadromous environments. Supporting this hypothesis, such collagen deposition due to cold acclimation was demonstrated to be reversible in rainbow trout, in which warm acclimation mimicking seasonal cycles reduces the collagen content (Johnston and Gillis 2022). Nevertheless, the possibility that, at least in part, cold exposure may contributes to the pronounced fibrotic response observed in *S. microcephalus* cannot be entirely excluded. Previous studies on the cardiocirculatory system of *S. microcephalus* have shown that it possesses a ventral aorta with a relatively low abundance of elastic fibers, which are loosely organized. This structural arrangement contributes to high arterial compliance at relatively low blood pressure (Shadwick et al. 2018). We hypothesize that age-related cardiac fibrosis in *S. microcephalus* may be functionally accommodated by the elastic properties of the ventral aorta, whose high compliance at low arterial pressure could mitigate the hemodynamic consequences of myocardial stiffening, a possibility that warrants direct functional testing.

Lipofuscin accumulation is widely regarded as a robust indicator of cellular aging, reflecting the progressive buildup of undegradable, cross-linked oxidized proteins and lipids within lysosomes of postmitotic cells (Terman and Brunk 1998, 2006; Brunk and Terman 2002). In this study, we report massive intracardiomyocyte deposition of lipofuscin in *S. microcephalus*, visualized using Sudan Black B staining, intrinsic autofluorescence, and photobleaching resistance. The signal was consistent across sexes and myocardial layers, while it is absent in the *E spinax*, suggesting that this is a generalized and pervasive feature in adult individuals of *S. microcephalus* species. Importantly, the persistent yellow-brown autofluorescence of lipofuscin in *S. microcephalus* and *N. furzeri* after photobleaching confirms its identity and highlights the robustness of the staining methods employed. Recently, metabolomic and proteomic analyzes of mouse hearts revealed elevated ROS levels in aged mice accompanied by a concomitant decline in antioxidant defenses, while lipidomic profiling showed a marked accumulation of lipids that may serve as precursors for lipofuscin formation (Basilicata et al. 2025). The extensive presence of lipofuscin-loaded autophagosomes and lysosomes in *S. microcephalus* cardiomyocytes evidenced by EM data, is consistent with a high tolerance to oxidative stress and impaired organelle turnover in the cardiac tissue. The accumulation of lipofuscin derived from damaged mitochondria indicates that, despite ongoing oxidative processes, these cells can maintain viability without activating excessive autophagy or undergoing apoptosis. This resilience may reflect an adaptive mechanism allowing long-lived species such as *S. microcephalus* to preserve cardiac function over extended lifespans.

The extent to which lipofuscin manifest in the heart of *S. microcephalus*, and whether such aging marker deposition differs from that observed in shorter-lived vertebrates, had not been previously explored. The confirmed accumulation of lipofuscin in *S. microcephalus* hearts underscores its significance as an aging marker and provides a valuable tool for investigating the biology of this exceptionally long-lived vertebrate. We did not have access to older individuals close to the species maximum size and it remains unknown whether lipofuscin accumulation and fibrosis plateaus in adult life or progress leading to an even starker phenotypes. Our analysis also revealed substantial deposition of 3-nitrotyrosine (3-NT) in the ventricular myocardium of *S. microcephalus*. As a well-established indicator of oxidative and nitrosative stress, 3-NT has been widely used to assess age-related redox imbalance in various tissues, including the heart. Age-associated increases in 3-NT have been documented in the cardiac tissue of several species, including the *N. furzeri* (Heid et al. 2017). In the present study

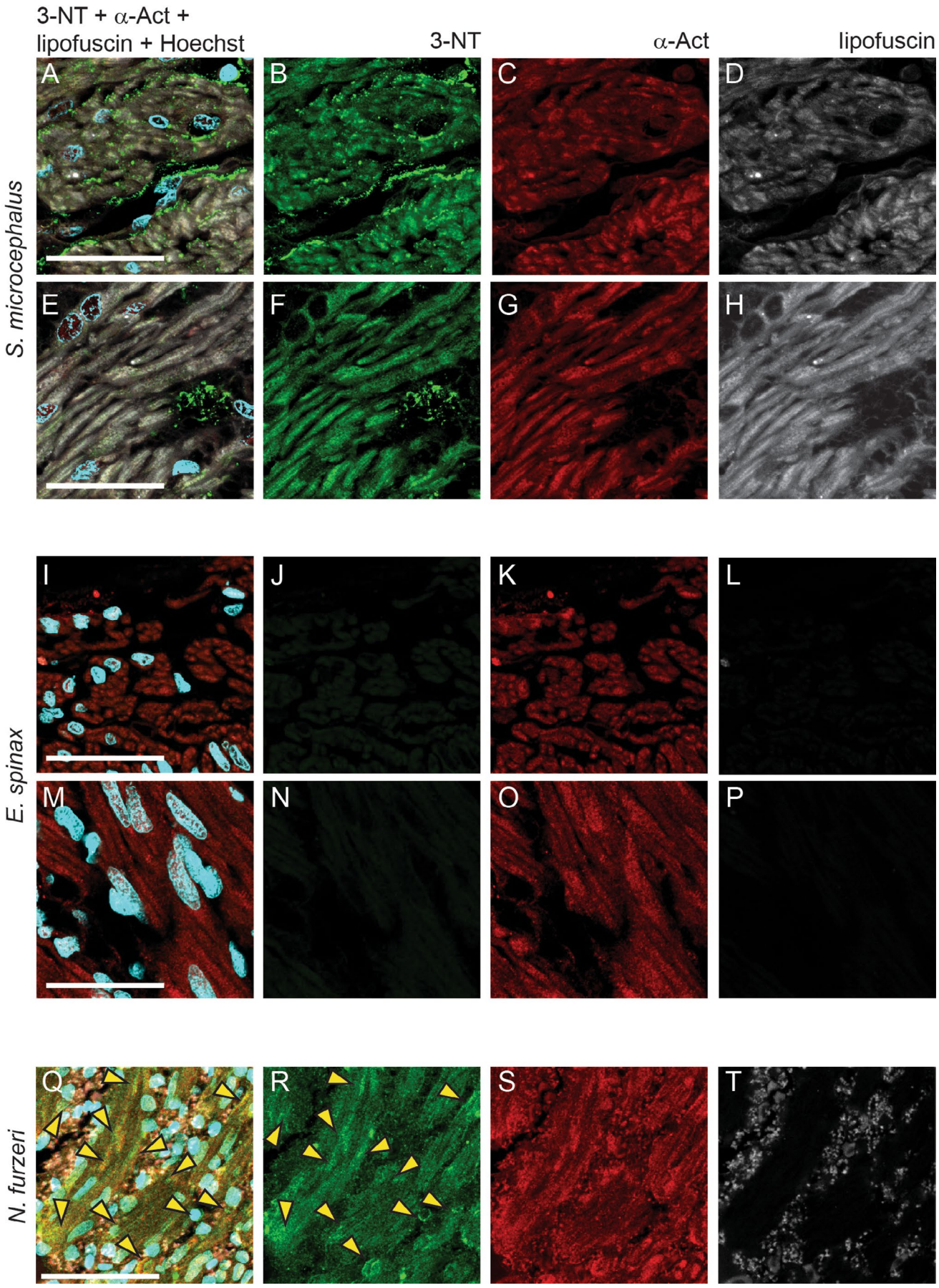

FIGURE 6 | Legend on next page.

FIGURE 6 | IHC showing 3-NT distribution in the ventricular myocardium. (A–D) *S. microcephalus* 341 cm TL female compact layer. (E–H) *S. microcephalus* 341 cm TL female spongy layer. (I–L) *E. spinax* female 300 mm TL compact layer. (M–P) *E. spinax* female 300 mm TL spongy layer. (Q–T) *N. furzeri* 39w old female cardiac ventricle myocardium. Yellow arrows: 3-NT accumulation. Scalebar 50 μm.

we were able to document the 3-NT in the myocardial tissue of *S. microcephalus*, while it proved to be absent in *E. spinax*. The spatial distribution of 3-NT immunoreactivity in *S. microcephalus* cardiomyocytes mirrored the pattern seen in aged *N. furzeri* heart, with further evident 3-NT deposits in the interstitial space of both compact and spongy layers. The oxidative stress theory of aging posits that longevity is achieved through reduced production of reactive oxygen species (ROS) or enhanced capacity to mitigate their effects. Yet, the case of *S. microcephalus* suggests an alternative model: that longevity may instead rely on exceptional resilience to chronic oxidative damage rather than its outright prevention. Supporting this notion, previous studies have reported high levels of oxidative status in the muscle of *S. microcephalus*, despite its remarkably long lifespan (Costantini et al. 2017) and mirrors the observation that naked mole rats show very high levels of lipid peroxidation as compared to mice (Andziak et al. 2006). Perhaps the most striking finding of this study is that, despite pronounced molecular and histological signatures of aging, *S. microcephalus* individuals appeared outwardly healthy and physiologically uncompromised at capture. This contrasts with mammalian models, where such features are typically associated with declining cardiac performance, increased arrhythmic risk, and mortality. The preservation of function despite accumulation of canonical aging markers, which are not detrimental for the century-living *S. microcephalus*, would suggest that the species tolerates its aged heart in a way that preserves function, however, direct functional evidence was not assessed in the present study and remains an important direction for future work. All together our findings raise the possibility that despite observable structural changes, *S. microcephalus* maintains effective cardiac function via compensatory mechanisms and extremely high resilience. This comparative approach offers a promising avenue to further uncover molecular and histological features that contribute to the remarkable physiological resilience of *S. microcephalus*, allowing its centenary long live. All together our data contribute foundational insight into how one of Earth's longest-lived vertebrates manages cellular and tissue aging in a vital organ. The *S. microcephalus* may illustrate a rare instance in which cumulative aging markers, such as fibrosis, lipofuscin and 3-NT, are tolerated, or perhaps compensated, without compromising cardiac function, offering a novel paradigm for understanding longevity in vertebrates. These findings may also inform translational approaches to mitigate age-related cardiac decline in humans.

Author Contributions

Elena Chiavacci: investigation, methodology, validation, conceptualization, formal analysis, visualization, writing – original draft, writing – review and editing. **Kirstine Fleng Steffensen**, **Emanuele Astoricchio**, **Amalie Bech Poulsen**, and **Daniel Brayson:** resources. **Pierre Delaroche:** investigation, methodology, validation, writing – review and editing. **Fulvio Garibaldi**, **Luca Lanteri**, **Giovanni Roppo Valente**, and **Federico Vignati:** resources, formal analysis, validation, writing – review and editing. **Christian Pinali:** validation, writing – review and editing. **John Fleng Steffensen** and **Holly Shiels:** resources, methodology, validation, writing – review and editing. **Eva Terzibasi Tozzini:** methodology, funding acquisition. **Alessandro Cellerino:** methodology, conceptualization, project administration, supervision, funding acquisition, visualization, writing – review and editing. All authors have read and agreed to the published version of the manuscript.

Acknowledgments

We are grateful to Dr. Sabine Matz and Dr. Cinzia Caterino for the support in the histological preparation of *N. furzeri* specimens. We also thank the staff of The University of Manchester Electron Microscopy Core Facility (RRID:SCR_021147; Faculty of Biology, Medicine and Health) for their assistance, particularly David Smith (former technician), whose support and expertise in SBF-SEM were instrumental in collecting these data. Open access publishing facilitated by Scuola Normale Superiore, as part of the Wiley - CRUI-CARE agreement.

Funding

This work was supported by the Italian Ministry of University and Research (MUR) [Funder ID: 10.13039/501100003407] under PRIN 2022—SHARKAGE (Grant number CUP: E53D23007660001) and the PNRR project "THE—Tuscany Health Ecosystem—Spoke 1 and Spoke 8." This work was supported by the Open Access Publishing Fund of the Scuola Normale Superiore.

Ethics Statement

Sampling in Greenland was carried out following laws and regulations and with authorization from the Government of Greenland (Ministry of Fisheries, Hunting & Agriculture, permit Nr. 2020–26,794 and 2023–6108 and document number 565466, 935119, 20,179,208, C-17-129, C-15-17, and C-13-16). Specimens of *E. spinax* were bycatch of commercial fisheries. *N. furzeri* were laboratory-bred as described by Naumann et al. (2024). All experiments were performed using the killifish strain MZM-0410 in accordance with relevant guidelines and regulations. Fish were bred and kept in the fish facility of the Leibniz Institute on Aging—Fritz Lipmann Institute according to §11 of the German Animal Welfare Act under license number J-003798. Sacrifice and organ harvesting were performed according to §4(3) of the German Animal Welfare Act.

Conflicts of Interest

The authors declare no conflicts of interest.

Data Availability Statement

Data sharing not applicable to this article as no datasets were generated or analysed during the current study.

References

Ahuja, G., D. Bartsch, W. Yao, et al. 2019. "Loss of Genomic Integrity Induced by Lysosphingolipid Imbalance Drives Ageing in the Heart." *EMBO Reports* 20: e47407.

Andziak, B., T. P. O'Connor, W. Qi, et al. 2006. "High Oxidative Damage Levels in the Longest-Living Rodent, the Naked Mole-Rat." *Aging Cell* 5: 463–471.

Anversa, P., and B. Nadal-Ginard. 2002. "Myocyte Renewal and Ventricular Remodelling." *Nature* 415: 240–243.

Aranha, A., G. Menezes, and M. R. Pinho. 2009. "Biological Aspects of the Velvet Belly Lantern Shark, *Etmopterus spinax* (Linnaeus, 1758) Off the Azores, North East Atlantic." *Marine Biology Research* 5: 257–267.

Basilicata, M. G., M. Malavolta, S. Marcozzi, et al. 2025. "Electron Microscopy and Multi-Omics Reveal Mitochondrial Dysfunction and Structural Remodeling in the Hearts of Elderly Mice." *Aging Cell* 24: e70286.

Biernacka, A., and N. G. Frangogiannis. 2011. "Aging and Cardiac Fibrosis." *Aging and Disease* 2: 158–173.

Brunk, U. T., and A. Terman. 2002. "Lipofuscin: Mechanisms of Age-Related Accumulation and Influence on Cell function12." *Free Radical Biology and Medicine* 33: 611–619.

Cardin, V., G. Civitarese, D. Hainbucher, M. Bensi, and A. Rubino. 2015. "Thermohaline Properties in the Eastern Mediterranean in the Last Three Decades: Is the Basin Returning to the Pre-EMT Situation?" *Ocean Science* 11: 53–66.

Cellerino, A., D. R. Valenzano, and M. Reichard. 2016. "From the Bush to the Bench: The Annual Nothobranchius Fishes as a New Model System in Biology." *Biological Reviews* 91: 511–533.

Chen, M. S., R. T. Lee, and J. C. Garbern. 2022. "Senescence Mechanisms and Targets in the Heart." *Cardiovascular Research* 118: 1173–1187.

Coelho, R., and K. Erzini. 2008. "Life History of a Wide-Ranging Deepwater Lantern Shark in the North-East Atlantic, *Etmopterus spinax* (Chondrichthyes: Etmopteridae), With Implications for Conservation." *Journal of Fish Biology* 73: 1419–1443.

Compagno, L. 1984. "FAO Species Catalogue. Vol. 4. Sharks of the World: An Annotated and Illustrated Catalogue of Shark Species Known to Date. Part 1. Hexanchiformes to Lamniformes." https://openknowledge.fao.org/items/e75adc48-defc-44ad-accd-9336eb4e5feb. Accessed July 21, 2025.

Compagno, L., M. Dando, and S. Fowler. 2005. "A Field Guide to the Sharks of the World." https://agris.fao.org/search/en/providers/122621/records/647396dae01106880098057d. Accessed July 21, 2025.

Costantini, D., S. Smith, S. S. Killen, J. Nielsen, and J. F. Steffensen. 2017. "The Greenland Shark: A New Challenge for the Oxidative Stress Theory of Ageing?" *Comparative Biochemistry and Physiology Part A: Molecular & Integrative Physiology* 203: 227–232.

Dai, D.-F., and P. S. Rabinovitch. 2009. "Cardiac Aging in Mice and Humans: The Role of Mitochondrial Oxidative Stress." *Trends in Cardiovascular Medicine* 19: 213–220.

Davies, S., M. H. Elliott, E. Floor, et al. 2001. "Photocytotoxicity of Lipofuscin in Human Retinal Pigment Epithelial Cells." *Free Radical Biology & Medicine* 31: 256–265.

Deerinck, T., E. Bushong, V. Lev-Ram, X. Shu, R. Tsien, and M. Ellisman. 2010. "Enhancing Serial Block-Face Scanning Electron Microscopy to Enable High Resolution 3-D Nanohistology of Cells and Tissues." *Microanalysis* 16: 1138–1139.

Di Cicco, E., E. T. Tozzini, G. Rossi, and A. Cellerino. 2011. "The Short-Lived Annual Fish *Nothobranchius furzeri* Shows a Typical Teleost Aging Process Reinforced by High Incidence of Age-Dependent Neoplasias." *Experimental Gerontology* 46: 249–256.

Farrell, A. P., A. M. Hammons, M. S. Graham, and G. F. Tibbits. 1988. "Cardiac Growth in Rainbow Trout, Salmo Gairdneri." *Canadian Journal of Zoology* 66: 2368–2373.

Fleg, J. L., and J. Strait. 2012. "Age-Associated Changes in Cardiovascular Structure and Function: A Fertile Milieu for Future Disease." *Heart Failure Reviews* 17: 545–554.

Follesa, C., and P. Carbonara, eds. 2019. "Atlas of Maturity Stages of Mediterranean Fishery Resources." https://policycommons.net/artifacts/1526159/atlas-of-the-maturity-stages-of-mediterranean-fishery-resources/2214270/. Accessed November 21, 2025.

Fukuda, R., A. Aharonov, Y. T. Ong, et al. 2019. "Metabolic Modulation Regulates Cardiac Wall Morphogenesis in Zebrafish." *eLife* 8: e50161.

Gazoti Debessa, C. R., L. B. Mesiano Maifrino, and R. Rodrigues de Souza. 2001. "Age Related Changes of the Collagen Network of the Human Heart." *Mechanisms of Ageing and Development* 122: 1049–1058.

Gennari, E., and U. Scacco. 2007. "First Age and Growth Estimates in the Deep Water Shark, *Etmopterus spinax* (Linnaeus, 1758), by Deep Coned Vertebral Analysis." *Marine Biology* 152: 1207–1214.

Goolish, E. M. 1987. "Cold-Acclimation Increases the Ventricle Size of Carp, *Cyprinus carpio*." *Journal of Thermal Biology* 12: 203–205.

Hansen, P. 1963. "Tagging Experiments With the Greenland Shark (*Somniosus microcephalus* (Bloch and Schneider)) in Subarea 1." *International Commission Northwest Atlantic Fisheries Special Publication* 4: 172–175.

Heid, J., C. Cencioni, R. Ripa, et al. 2017. "Age-Dependent Increase of Oxidative Stress Regulates microRNA-29 Family Preserving Cardiac Health." *Scientific Reports* 7: 16839.

Herbert, N. A., P. V. Skov, B. Tirsgaard, et al. 2017. "Blood O2 Affinity of a Large Polar Elasmobranch, the Greenland Shark *Somniosus microcephalus*." *Polar Biology* 40: 2297–2305.

Houpert, L., P. Testor, X. Durrieu de Madron, et al. 2015. "Seasonal Cycle of the Mixed Layer, the Seasonal Thermocline and the Upper-Ocean Heat Storage Rate in the Mediterranean Sea Derived From Observations." *Progress in Oceanography* 132: 333–352.

Johnston, E. F., and T. E. Gillis. 2022. "Regulation of Collagen Deposition in the Trout Heart During Thermal Acclimation." *Current Research in Physiology* 5: 99–108.

Kakimoto, Y., C. Okada, N. Kawabe, et al. 2019. "Myocardial Lipofuscin Accumulation in Ageing and Sudden Cardiac Death." *Scientific Reports* 9: 3304.

Kane, A. E., E. S. Bisset, S. Heinze-Milne, K. M. Keller, S. A. Grandy, and S. E. Howlett. 2021. "Maladaptive Changes Associated With Cardiac Aging Are Sex-Specific and Graded by Frailty and Inflammation in C57BL/6 Mice." *Journals of Gerontology: Series A* 76: 233–243.

Keen, A. N., A. J. Fenna, J. C. McConnell, M. J. Sherratt, P. Gardner, and H. A. Shiels. 2015. "The Dynamic Nature of Hypertrophic and Fibrotic Remodeling of the Fish Ventricle." *Frontiers in Physiology* 6: 427.

Kelmer Sacramento, E., J. M. Kirkpatrick, M. Mazzetto, et al. 2020. "Reduced Proteasome Activity in the Aging Brain Results in Ribosome Stoichiometry Loss and Aggregation." *Molecular Systems Biology* 16: e9596.

Kent, J., M. Koban, and C. L. Prosser. 1988. "Cold-Acclimation-Induced Protein Hypertrophy in Channel Catfish and Green Sunfish." *Journal of Comparative Physiology. B* 158: 185–198.

Knyushko, T. V., V. S. Sharov, T. D. Williams, C. Schöneich, and D. J. Bigelow. 2005. "3-Nitrotyrosine Modification of SERCA2a in the Aging Heart: A Distinct Signature of the Cellular Redox Environment." *Biochemistry* 44: 13071–13081.

König, J., C. Ott, M. Hugo, et al. 2017. "Mitochondrial Contribution to Lipofuscin Formation." *Redox Biology* 11: 673–681.

Kremer, J. R., D. N. Mastronarde, and J. R. McIntosh. 1996. "Computer Visualization of Three-Dimensional Image Data Using IMOD." *Journal of Structural Biology* 116: 71–76.

Lai, N. C., K. E. Korsmeyer, S. Katz, D. B. Holts, L. M. Laughlin, and J. B. Graham. 1997. "Hemodynamics and Blood Properties of the Shortfin Mako Shark (*Isurus oxyrinchus*)." *Copeia* 1997: 424–428.

Le Mével, J.-C., N. Mimassi, F. Lancien, D. Mabin, J.-M. Boucher, and J.-J. Blanc. 2002. "Heart Rate Variability, a Target for the Effects of Angiotensin II in the Brain of the Trout *Oncorhynchus mykiss*." *Brain Research* 947: 34–40.

Lesnefsky, E. J., Q. Chen, and C. L. Hoppel. 2016. "Mitochondrial Metabolism in Aging Heart." *Circulation Research* 118: 1593–1611.

Levy, D., K. M. Anderson, D. D. Savage, W. B. Kannel, J. C. Christiansen, and W. P. Castelli. 1988. "Echocardiographically Detected Left Ventricular Hypertrophy: Prevalence and Risk Factors." *Annals of Internal Medicine* 108: 7–13.

López-Unzu, M. A., M. Teresa Soto-Navarrete, V. Sans-Coma, B. Fernández, and A. Carmen Durán. 2024. "The Myoarchitecture of the Vertebrate Cardiac Ventricles: Evolution and Classification." *Journal of Experimental Biology* 227: jeb247441.

Lu, J.-Q., C. M. F. Monaco, T. J. Hawke, C. Yan, and M. A. Tarnopolsky. 2020. "Increased Intra-Mitochondrial Lipofuscin Aggregates With Spherical Dense Body Formation in Mitochondrial Myopathy." *Journal of the Neurological Sciences* 413: 30152.

Lu, L., J. Guo, Y. Hua, et al. 2017. "Cardiac Fibrosis in the Ageing Heart: Contributors and Mechanisms." *Clinical and Experimental Pharmacology and Physiology* 44: 55–63.

Ma, X., Y. Ding, D. Mondaca-Ruff, et al. 2025. "*Nothobranchius furzeri*: A Vertebrate Model for Studying Cardiac Aging and Cellular Senescence." *Npj Aging* 11: 63.

MacNeil, M. A., M. M. BC, N. E. Hussey, et al. 2012. "Biology of the Greenland Shark *Somniosus microcephalus*." *Journal of Fish Biology* 80: 991–1018.

Malkoff, D. B., and B. L. Strehler. 1963. "The Ultrastructure of Isolated and In Situ Human Cardiac Age Pigment." *Journal of Cell Biology* 16: 611–616.

Naumann, U., J. L. Brazzell, M. J. Crim, and B. Hoppe. 2024. "Comprehensive Colony Health Management and Emerging Pathogens of the Annual Killifish Species *Nothobranchius furzeri*." *Journal of the American Association for Laboratory Animal Science* 63: 20–33.

Ng'oma, E., K. Reichwald, A. Dorn, et al. 2014. "The Age Related Markers Lipofuscin and Apoptosis Show Different Genetic Architecture by QTL Mapping in Short-Lived Nothobranchius Fish." *Aging (Albany NY)* 6: 468–480.

Nielsen, J., R. B. Hedeholm, J. Heinemeier, et al. 2016. "Eye Lens Radiocarbon Reveals Centuries of Longevity in the Greenland Shark (*Somniosus microcephalus*)." *Science* 353: 702–704.

Perry, S. F., R. Fritsche, T. M. Hoagland, D. W. Duff, and K. R. Olson. 1999. "The Control of Blood Pressure During External Hypercapnia in the Rainbow Trout (*Oncorhynchus mykiss*)." *Journal of Experimental Biology* 202: 2177–2190.

Pinali, C., and A. Kitmitto. 2014. "Serial Block Face Scanning Electron Microscopy for the Study of Cardiac Muscle Ultrastructure at Nanoscale Resolutions." *Journal of Molecular and Cellular Cardiology* 76: 1–11.

Ronneberger, O., P. Fischer, and T. Brox. 2015. "U-Net: Convolutional Networks for Biomedical Image Segmentation." In *Medical Image Computing and Computer-Assisted Intervention – MICCAI 2015*, edited by N. Navab, J. Hornegger, W. M. Wells, and A. F. Frangi, 234–241. Springer International Publishing.

Sánchez-Iranzo, H., M. Galardi-Castilla, C. Minguillón, et al. 2018. "Tbx5a Lineage Tracing Shows Cardiomyocyte Plasticity During Zebrafish Heart Regeneration." *Nature Communications* 9: 428.

Schulman, S. P., E. G. Lakatta, J. L. Fleg, L. Lakatta, L. C. Becker, and G. Gerstenblith. 1992. "Age-Related Decline in Left Ventricular Filling at Rest and Exercise." *American Journal of Physiology. Heart and Circulatory Physiology* 263: H1932–H1938.

Shadwick, R. E., D. Bernal, P. G. Bushnell, and J. F. Steffensen. 2018. "Blood Pressure in the Greenland Shark as Estimated From Ventral Aortic Elasticity." *Journal of Experimental Biology* 221: jeb186957.

Smith, D., and T. Starborg. 2019. "Serial Block Face Scanning Electron Microscopy in Cell Biology: Applications and Technology." *Tissue and Cell* 57: 111–122.

Ste-Marie, E., Y. Y. Watanabe, J. M. Semmens, M. Marcoux, and N. E. Hussey. 2022. "Life in the Slow Lane: Field Metabolic Rate and Prey Consumption Rate of the Greenland Shark (*Somniosus microcephalus*) Modelled Using Archival Biologgers." *Journal of Experimental Biology* 225: jeb242994.

Straube, N., C. Li, J. M. Claes, S. Corrigan, and G. J. P. Naylor. 2015. "Molecular Phylogeny of Squaliformes and First Occurrence of Bioluminescence in Sharks." *BMC Evolutionary Biology* 15: 162.

Sun, Y., and A. Chakrabartty. 2016. "Cost-Effective Elimination of Lipofuscin Fluorescence From Formalin-Fixed Brain Tissue by White Phosphor Light Emitting Diode Array." *Biochemistry and Cell Biology* 94: 545–550.

Taylor, J. S., I. Braasch, T. Frickey, A. Meyer, and Y. Van de Peer. 2003. "Genome Duplication, a Trait Shared by 22,000 Species of Ray-Finned Fish." *Genome Research* 13: 382–390.

Terman, A., and U. T. Brunk. 1998. "Lipofuscin: Mechanisms of Formation and Increase With Age." *APMIS* 106: 265–276.

Terman, A., and U. T. Brunk. 2006. "Oxidative Stress, Accumulation of Biological 'Garbage', and Aging." *Antioxidants & Redox Signaling* 8: 197–204.

Terman, A., H. Dalen, J. W. Eaton, J. Neuzil, and U. T. Brunk. 2004. "Aging of Cardiac Myocytes in Culture: Oxidative Stress, Lipofuscin Accumulation, and Mitochondrial Turnover." *Annals of the New York Academy of Sciences* 1019: 70–77.

Terzibasi, E., C. Lefrançois, P. Domenici, N. Hartmann, M. Graf, and A. Cellerino. 2009. "Effects of Dietary Restriction on Mortality and Age-Related Phenotypes in the Short-Lived Fish *Nothobranchius furzeri*." *Aging Cell* 8: 88–99.

Terzibasi, E., D. R. Valenzano, M. Benedetti, et al. 2008. "Large Differences in Aging Phenotype Between Strains of the Short-Lived Annual Fish *Nothobranchius furzeri*." *PLoS One* 3: e3866.

Terzibasi Tozzini, E., A. Dorn, E. Ng'oma, et al. 2013. "Parallel Evolution of Senescence in Annual Fishes in Response to Extrinsic Mortality." *BMC Evolutionary Biology* 13: 77.

Timmis, A., V. Aboyans, P. Vardas, et al. 2024. "European Society of Cardiology: The 2023 Atlas of Cardiovascular Disease Statistics." *European Heart Journal* 45: 4019–4062.

Townsend, N., D. Kazakiewicz, F. Lucy Wright, et al. 2022. "Epidemiology of Cardiovascular Disease in Europe." *Nature Reviews. Cardiology* 19: 133–143.

Visseren, F. L. J., F. Mach, Y. M. Smulders, et al. 2021. "2021 ESC Guidelines on Cardiovascular Disease Prevention in Clinical Practice." *European Heart Journal* 42: 3227–3337.

Vlachopoulos, C., K. Aznaouridis, and C. Stefanadis. 2010. "Prediction of Cardiovascular Events and All-Cause Mortality With Arterial Stiffness: A Systematic Review and Meta-Analysis." *Journal of the American College of Cardiology* 55: 1318–1327.

Wang, L., C.-Y. Xiao, J.-H. Li, G.-C. Tang, and S.-S. Xiao. 2022. "Transport and Possible Outcome of Lipofuscin in Mouse Myocardium." *Advances in Gerontology* 12: 247–263.

Watanabe, Y. Y., C. Lydersen, A. T. Fisk, and K. M. Kovacs. 2012. "The Slowest Fish: Swim Speed and Tail-Beat Frequency of Greenland Sharks." *Journal of Experimental Marine Biology and Ecology* 426–427: 5–11.

Yoneyama, K., B. A. Venkatesh, D. A. Bluemke, R. L. McClelland, and J. A. C. Lima. 2016. "Cardiovascular Magnetic Resonance in an Adult Human Population: Serial Observations From the Multi-Ethnic Study of Atherosclerosis." *Journal of Cardiovascular Magnetic Resonance* 19: 52.

Supporting Information

Additional supporting information can be found online in the Supporting Information section. **Figure S1:** Representative of *S. microcephalus* ventricular wall. Black arrow: pericardial fibrotic capsule. Yellow arrow: compact myocardial layer. Green arrow: spongy myocardial layer. Yellow asterisks: coronary vessels. Blue scalebar: 500 μm. **Figure S2:** Representatives of *S. microcephalus* coronary cardiac fibrosis, green arrows: (A) female 341 cm; (B) female 341 cm; (C) male 310 cm. **Figure S3:** Representative examples of the (A) total tissue mask, (B) collagen mask, (C) overlay mask of *Somniosus microcephalus* (sample 7). Fibrosis percentage ratio is expressed as % (collagen/total area) as described in Materials and Methods section. Scalebar: 100 μm. **Figure S4:** Analysis of the 390 TL *S. microcephalus* specimen. Masson's trichrome staining of (A) compact and (B) spongy myocardial layer. Sudan black B of (C) compact and (D) spongy layer. Native lipofuscin of (E) compact and (F) spongy layer. IHC showing lysosomes and lipofuscin accumulation acquired with Airyscan: (G–J) compact and (K–N) spongy myocardial layer. Orange arrows: single examples of lysosomal Lamp1 and lipofuscin colocalization. Purple arrows: single examples of lipofuscin granules. Cyan: Hoechst. Green: Lamp1. White: lipofuscin. Black scalebar: 100 μm. White scalebar: 50 μm. **Table S1:** acel70505-sup-0002-TableS1.pdf. *S. microcephalus* parametres. F, female; M, male; IHC, immunohistochemistry Lamp1; EM, Electron Microscopy; N/A, Not Applicable. **Table S2:** acel70505-sup-0003-TableS2.pdf. *E. spinax* parametres. F, female; M, male. **Video S1:** Autophagosome reconstruction. Blue: autophagosome. Pink: mitochondria.